Effects of Torsional Dynamics on Nonlinear Generator Control

Eric H. Allen, Jeff W. Chapman, and Marija D. Ilić

Abstract—**The performance of a feedback-linearizing control for excitation control of a synchronous generator is investigated with respect to unmodeled dynamics of both the turbine generator unit and the transmission network. It is found that certain types of dynamics that were not modeled during the design of the control enter in a manner that does affect the performance of the control, but that preserves the linearity of the closed-loop system. Moreover, the control acts to decouple the dynamics associated with the machine from the dynamics of the transmission grid, thus preventing subsynchronous resonance between the two subsystems when a series capacitor is used to compensate the transmission line. The stability robustness of the feedback-linearizing control is investigated with respect to a structured uncertainty. The uncertainty considered corresponds to the spring modes of the generator shaft and enters in such a way that analysis by Kharitonov's theorem is feasible. It is shown that the control remains stable over a wide range of values of the shaft parameters. A sliding control is designed and compared to the feedback-linearizing control with respect to performance degradation for this type of uncertainty, and it is found that, because of the tight saturation limits on the control signal, the sliding control offers no discernable performance advantage for this type of structured uncertainty.**

I. Introduction

RECENTLY, feedback-linearizing controls (FBLC's) have been proposed for excitation control of synchronous electric generators [1], [2]. These designs have shown promise in simulations, but they require a measurement of the angular acceleration of the generator shaft. More detailed studies of the unmodeled dynamics are required, particularly as they impact the performance and the stability robustness of the controller. Two different classes of unmodeled dynamics are considered: 1) the unmodeled dynamics of the turbine-generator subsystem and 2) the electromagnetic dynamics of the transmission grid.

The first type is typically ignored, based on a heuristic time-scale separation argument which can be shown to be false through an application of singular perturbation theory. Interestingly, however, the unmodeled shaft interaction enters in such a way that the behavior of the feedback-linearized system remains linear. Thus the results reported here may be applicable to systems with a similar type of uncertainty.

The second type of unmodeled dynamics also is typically ignored, based on time-scale separation, but must be considered to capture the important phenomenon of subsynchronous resonance which is a resonance of the natural modes of the torsional subsystem with the transmission grid. Subsynchronous resonance is typically associated with the use of series capacitor compensation on transmission lines. In 1970, unstable subsynchronous oscillations resulted in two shaft failures at the Mohave generating station in Nevada; this event illustrated the fact that the torsional dynamics of the generator shaft may interact with oscillatory currents in the transmission grid via the magnetic fields in the generator air gap [3].

From a theoretical viewpoint, the paper provides an example of a dynamical model for which it is not justifiable to neglect higher-order dynamics, even though in this case the natural shaft modes are over a decade faster than the nominal poles of the controller. This is shown using both singular perturbation and the selective modal analysis (SMA). On the other hand, if these dynamics are included in the design of the FBLC, unacceptably high control amplitudes result. Because of this, one proceeds with the design in which the shaft modes are neglected. The impact of this on controller performance is shown.

The synchronous generator application also places severe limits on the allowable magnitude of the control signal. Therefore extensive simulations are required to verify that the system response to control saturation is benign. The presence of a large torsional "ripple" on the acceleration measurement severely aggravates the control saturation problem. One possible method for limiting saturation is field voltage averaging and/or filtering of the acceleration measurement. Results show that these methods are capable of improving FBLC performance, but the averaging or filtering can also cause instability.

With respect to the transmission elements, FBLC is shown to decouple these dynamics from the torsional dynamics of the generator. This separation prevents the interaction that can produce an undesired resonance.

It is known that an FBLC is not generically robust to uncertainty, and therefore care must be exercised in evaluating the effects of unmodeled dynamics on the control design. In the example of FBLC of the excitation of a synchronous electric generator, it was found that a certain class of dynamics (specifically, the shaft dynamics) that are customarily ignored in the control design enter in such a way that, although the design poles of the FBLC are shifted, the closed-loop system remain linear. For the particular example considered, this composite system was shown to be stable. It is important, however, to verify that the composite system will remain stable if the parameters of the shaft dynamics vary, since

Manuscript received March 6, 1995. Recommended by Associate Editor, R. Ravi.

The authors are with the Department of Electrical Engineering and Computer Science, Massachusetts Institute of Technology, Cambridge, MA 02139 USA.

Publisher Item Identifier S 1063-6536(96)02071-4.

these parameters are not normally known with good precision. This is a case of structured uncertainty, since the form of the model is assumed to be known, but the parameters are uncertain. Because the linearity of the system is preserved for this particular case, there are several methods available for evaluating the robustness of the controller with respect to parameter uncertainty.

Clearly there are a multitude of uncertainties in addition to the shaft parameters, and as noted earlier, FBLC is not considered to be a robust methodology. Therefore it may be desirable to use a control methodology that allows for a more general class of uncertainty. One such control scheme is sliding mode control. In this method, the system state is confined, after a finite "reaching" interval, to evolve ("slide") upon a manifold that is specified as part of the design. Typically, the manifold is chosen such that the evolution of system trajectories is linear. In this paper we develop a sliding control design whose trajectories correspond to the original FBLC design. The response of the design should then be similar to FBLC, but the robustness to model uncertainties is well established.

This paper is organized in the following way: The first part examines the closed-loop system performance in the presence of unmodeled turbine/generator dynamics, neglecting the transmission line dynamics. Once all conclusions are drawn for this case, the problem is revisited with explicit consideration of transmission line dynamics. Both problems are of practical importance. Next, the robustness of the controller to variations in the shaft parameters is examined. Finally, a sliding mode controller is designed, and its performance in the presence of the shaft dynamics is compared to that of FBLC.

II. Development of FBLC

The FBLC is designed for a fourth-order generator model with state vector $\mathbf{x}_g = [\delta\ \omega\ E'_q\ E'_d]^T$. Only three states (δ, ω, E'_q) can be feedback linearized; by means of a state vector transformation, we may write the dynamics of these three states in Brunovsky form with $\mathbf{z} = [(\delta-\delta_o)\ (\omega-\omega_o)\ \alpha]^T$ [1]

$$\dot{\delta} = \omega - \omega_o \tag{1}$$

$$\dot{\omega} = \alpha \tag{2}$$

$$\dot{\alpha} = \rho(\mathbf{x}_g) + \beta(\mathbf{x}_g)E_{fd} \tag{3}$$

$$\begin{aligned}\rho(\mathbf{x}_g) = &-\frac{\omega_o}{2H}\left[D\frac{\dot{\omega}}{\omega_o} + \dot{E}'_d i_d + E'_d \dot{i}_d + \dot{E}'_q i_q \right.\\ &\left. - E'_q \frac{\partial i_q}{\partial E'_q}\dot{E}'_q - E'_d \frac{\partial i_d}{\partial E'_q}\dot{E}'_q\right]\\ &+ \frac{\omega_o}{2HT'_{d0}}[E'_q + (x_d - x'_d)i_d]\\ &\cdot\left[E'_q \frac{\partial i_q}{\partial E'_q} + E'_d \frac{\partial i_d}{\partial'_q} + i_q\right]\end{aligned} \tag{4}$$

$$\beta(\mathbf{x}_g) = -\frac{\omega_o}{2HT'_{d0}}\left[E'_q \frac{\partial i_q}{\partial E'_q} + E'_d \frac{\partial i_d}{\partial E'_d} + i_q\right]. \tag{5}$$

Upon applying the following signal to the field voltage

$$E_{fd} = \frac{\mathbf{a}^T\mathbf{z} - \rho(\mathbf{x}_g)}{\beta(\mathbf{x}_g)} \tag{6}$$

where $\mathbf{a} = [a_0\ a_1\ a_2]^T$, these dynamics of the generator will be linear, according to [1]

$$\dot{\delta} = \omega - \omega_o \tag{7}$$

$$\dot{\omega} = \alpha \tag{8}$$

$$\dot{\alpha} = a_0(\delta - \delta_o) + a_1(\omega - \omega_o) + a_2\alpha. \tag{9}$$

The FBLC was tested with all three poles at -5; to achieve this, one sets $a_0 = -125$, $a_1 = -75$, and $a_2 = -15$. This choice of pole locations is approximately one decade below the slowest unmodeled dynamics in the system.

As noted in Section I, E_{fd} has maximum and minimum saturation limits. If the calculated E_{fd} from the controller exceeds these limits, the actual field voltage remains at the limit value. For this paper, E_{fd} is constrained between 0 and 6.16 pu. The use of a smaller range for E_{fd} was also investigated, but no qualitative change in the results was observed.

III. Effects of Unmodeled Dynamics of the Generator

When considering the torsional dynamics, the model assumes the form

$$\begin{bmatrix}\dot{\mathbf{z}}\\ \dot{\mathbf{x}}_1\end{bmatrix} = \begin{bmatrix}\mathbf{A}_{11} & \mathbf{A}_{12}\\ \mathbf{A}_{21} & \mathbf{A}_{22}\end{bmatrix}\begin{bmatrix}\mathbf{z}\\ \mathbf{x}_1\end{bmatrix}. \tag{10}$$

Notice that the shaft subsystem, represented by the vector $\mathbf{x}_1$, is linear, and the combined system remains linear even in the presence of the additional dynamics. This situation holds for the example in this paper, although it is not generally true for all types of unmodeled dynamics.

FBLC design, intended to produce (7)–(9), actually results in (10). Consequently, there is a significant change in the quality of the system response. The closed-loop pole placement differs from the original design. The field voltage saturates frequently, since $\mathbf{x}_1$ is strongly coupled to z_3. The damping of $\mathbf{x}_1$ is much greater, however, in the combined model than the natural damping of the isolated shaft model.

This is an unusual example because the coupling between $\mathbf{z}$ and $\mathbf{x}_1$ is strong; i.e., $\|\mathbf{A}_{12}\|$ and $\|\mathbf{A}_{21}\|$ are greater than or equal to $\|\mathbf{A}_{11}\|$ and $\|\mathbf{A}_{22}\|$. Therefore, the standard singular perturbations argument does not hold for this model; $\mathbf{x}_1$ are not "faster" variables than $\mathbf{z}$ [4]. Applying SMA to this problem yields the same conclusion [5]. Note that SMA was used in [7] on a system with subsynchronous resonance; however, in that example, the shaft states were retained in the reduced-order model.

FBLC requires a measurement of z_3, which is greatly affected by $\mathbf{x}_1$, resulting in control saturation. Several approaches to handling the saturation problem are considered. One possibility is averaging the control input u; however, straightforward averaging of u does not assure stability. The same problem occurs if low-pass filtering of z_3 is used, although in some cases this technique is able to significantly reduce saturation and improve FBLC performance. Another

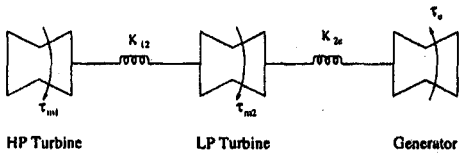

Fig. 1. The torsional spring-mass model.

approach is to modify $\rho(\mathbf{z})$ and $\beta(\mathbf{z})$ to include the effects of $\mathbf{x}_1$. Unfortunately, this method increases the control saturation and further degrades the performance.

If no modifications are made to FBLC, then good pole placement is achieved for $\mathbf{z}$, even in the presence of $\mathbf{x}_1$. The only drawback is that rail-to-rail control switching at the frequency of the shaft modes (usually 10 to 50 Hz) is observed. In the small disturbance case, the performance of FBLC with respect to the dynamics of $\mathbf{z}$ is not seriously degraded, despite the fact that $\|\mathbf{A}_{12}\|$ is large.

IV. Model of Generator/Shaft Turbine

Fig. 1 shows a typical shaft in a power generator. The generator, turbine, and shaft are commonly modeled as a series of rotating masses connected by torsional springs. Each mass also experiences damping torques. The inertia constants of the two turbines will be denoted as H_1 and H_2, while the generator constant will be referred to as H_e. The shaft model is then taken as a sixth-order linear system [5], [8]

$$\frac{2H_1}{\omega_o}\frac{d^2\delta_1}{dt^2} = P_{1u} - D_{1u}\frac{\dot{\omega}_1}{\omega_o} - K_{12u}\frac{\delta_1 - \delta_2}{\omega_o} \tag{11}$$

$$\frac{2H_2}{\omega_o}\frac{d^2\delta_2}{dt^2} = P_{2u} - D_{2u}\frac{\omega_2}{\omega_o} - K_{12u}\frac{\delta_2 - \delta_1}{\omega_o} - K_{2eu}\frac{\delta_2 - \delta_e}{\omega_o} \tag{12}$$

$$\frac{2H_e}{\omega_o}\frac{d^2\delta_e}{dt^2} = -P_{eu} - D_{eu}\frac{\omega_e}{\omega_o} - K_{2eu}\frac{\delta_e - \delta_2}{\omega_o} \tag{13}$$

where δ_i and $\omega_i = \dot{\delta}_i$ represent, respectively, the angle and speed of mass i. Notice that $\delta = \delta_e$ and $\omega = \omega_e$ are the common states that couple the shaft and the generator.

A. Sample Torsional Shaft Model

The parameters for the example model in this paper are the same as used in [5]

$$\begin{array}{lll} H_1 = 0.3474\text{s} & K_{12u} = 20158\text{s}^{-1} & D_{1u} = 0.08869 \\ H_2 = 1.9927\text{s} & K_{2eu} = 40219\text{s}^{-1} & D_{2u} = 0.5521 \\ H_e = 1.160\text{s} & & D_{eu} = 0.3131. \end{array} \tag{14}$$

The eigenvalues of the shaft system, given the shaft parameters above, appear in Table I. In this case, the shaft modes are at 24.07 and 31.28 Hz. This places the shaft modes well within the typical range of 10–50 Hz [8].

V. The Combined Generator and Shaft Model

The feedback linearizing controller derivation was based on a fourth-order generator model. This model assumes that

$$\dot{\omega} = \frac{\omega_o}{2H}\left[P_m - D\frac{\omega}{\omega_o} - E'_d i_d - E'_q i_q\right] \tag{15}$$

TABLE I
Eigenvalues and Frequencies of the Torsional State-Space Shaft Model

Number(s)	Eigenvalue	Frequency (Hz)
1,2	$-0.07 \pm j196.54$	31.28
3,4	$-0.07 \pm j151.24$	24.07
5	0.00	–
6	−0.14	–

where $H = H_1 + H_2 + H_e$ represents the combined rotational inertia of the turbines and generator, and P_m is the mechanical power from the turbines which is treated as a constant. When torsional dynamics are included, however, the equation for $\dot{\omega}$ is taken from (13)

$$\dot{\omega} = \dot{\omega}_e = \frac{\omega_o}{2H_e}\left[K_{2eu}\frac{\delta_2}{\omega_o} - K_{2eu}\frac{\delta_e}{\omega_o} - D_{eu}\frac{\omega_e}{\omega_o} - E'_d i_d - E'_q i_q\right] \tag{16}$$

given that $P_{eu} = E'_d i_d + E'_q i_q$. If we differentiate (16), following the same procedure used in [1] and [2], we find that

$$\dot{\alpha} = \rho_t(\mathbf{x}_g) + \beta_t(\mathbf{x}_g)E_{fd} \tag{17}$$

where

$$\begin{aligned}\rho_t(\mathbf{x}_g) = -\frac{\omega_o}{2H_e}\Bigg[&-K_{2eu}\frac{\omega_2}{\omega_o} + K_{2eu}\frac{\omega_e}{\omega_o} + D_{eu}\frac{\dot{\omega}_e}{\omega_o} \\ &+ \dot{E}'_d i_d + E'_d \dot{i}_d + \dot{E}'_q i_q - E'_q \frac{\partial i_q}{\partial E'_q}\dot{E}'_q - E'_d \frac{\partial i_d}{\partial E'_q}\dot{E}'_q\Bigg] \\ &+ \frac{\omega_o}{2H_e T'_{d0}}[E'_q + (x_d - x'_d)i_d] \\ &\cdot\left[E'_q \frac{\partial i_q}{\partial E'_q} + E'_d \frac{\partial i_d}{\partial E'_q} + i_q\right]\end{aligned} \tag{18}$$

$$\beta_t(\mathbf{x}_g) = -\frac{\omega_o}{2H_e T'_{d0}}\left[E'_q \frac{\partial i_q}{\partial E'_q} + E'_d \frac{\partial i_d}{\partial E'_q} + i_q\right]. \tag{19}$$

Thus, when the feedback signal defined in (6) is applied (i.e., when the control based on the simpler model is used), the generator-shaft system is still linearized, although $\dot{\alpha}$ picks up some extra terms

$$\dot{\alpha} = \frac{H}{H_e}\mathbf{a}^T\mathbf{z} - \frac{\omega_o}{2H_e}\left[-K_{2eu}\frac{\omega_2}{\omega_o} + K_{2eu}\frac{\omega_e}{\omega_o} + D_{eu}\frac{\dot{\omega}_e}{\omega_o} - D\frac{\dot{\omega}_e}{\omega_o}\right]. \tag{20}$$

Three generator states, δ, ω, α and the four shaft states, δ_1, ω_1, δ_2, ω_2, form a seventh-order linear system when FBLC is used. The eigenvalues of this system, given the same controller and shaft parameters as before, are shown in Table II. Notice that the torsional modes are still present at 24 and 31 Hz, but the damping of these modes has improved significantly. Additionally, the poles which were nominally located at -5 have shifted, giving rise to a strongly damped conjugate pair of 0.17 Hz.

Note that the real part of the eigenvalues of Table II are all of the same order of magnitude. This suggests that time-scale separation does not hold for the generator and shaft

TABLE II
EIGENVALUES AND FREQUENCIES OF THE SHAFT/GENERATOR MODEL WITH FEEDBACK LINEARIZING CONTROL

Number(s)	Eigenvalue	Frequency (Hz)
1	-6.99	-
2,3	$-4.12 \pm j1.04$	0.1662
4,5	$-2.69 \pm j195.55$	31.12
6,7	$-12.52 \pm j150.52$	23.96

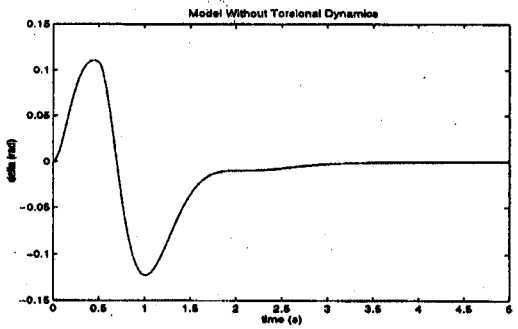

Fig. 2. Response of $\delta - \delta_o$ to a 0.5 s fault without torsional modeling.

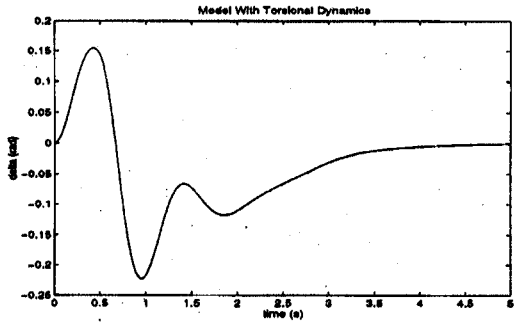

Fig. 3. Response of $\delta - \delta_o$ to a 0.5 s fault with torsional modeling. The torsional dynamics affect the response of δ, although δ still returns to equilibrium within a reasonable time.

dynamics. This can be rigorously confirmed by using selective modal analysis to calculate the participation factors [4], [6]. Therefore, both sets of dynamics must be retained when analyzing FBLC performance in the presence of torsional oscillations on the shaft.

VI. FIELD VOLTAGE SATURATION

Figs. 2–7 illustrate the impact of the shaft dynamics on an FBLC-equipped machine. A sixth-order generator model similar to [9] is used for these simulations and all others in this paper. The large swings in E_{fd} primarily result from the high-frequency oscillations present in the shaft acceleration measurement. Notice in Fig. 5 that the amplitude of the high-frequency oscillations in $\dot{\omega}$ is about 6 rad/s^2 at $t = 0.5$ s. Since E_{fd} includes the acceleration measurement multiplied

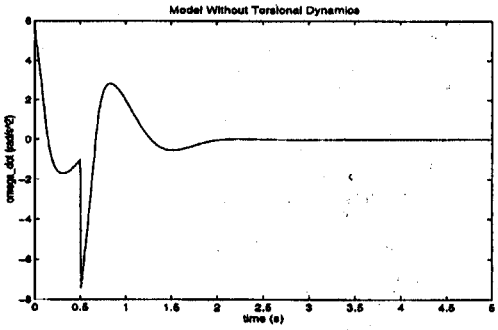

Fig. 4. Response of $\dot{\omega}$ to a 0.5 s fault without torsional modeling.

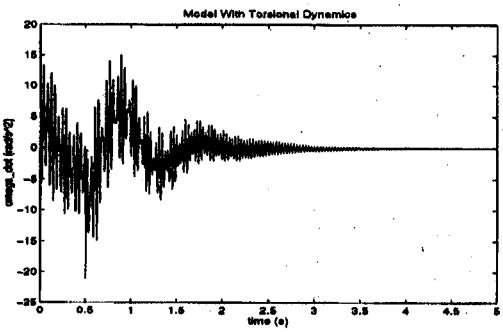

Fig. 5. Response of $\dot{\omega}$ to a 0.5 s fault with torsional modeling. The shaft oscillations form a large portion of the acceleration measurement.

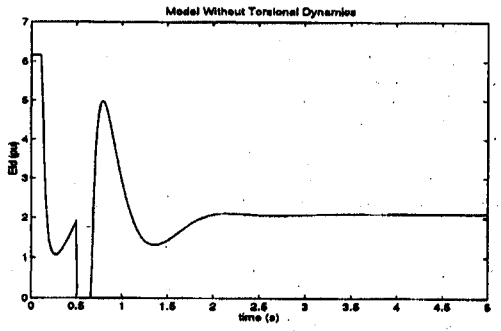

Fig. 6. Response of E_{fd} to a 0.5 s fault without torsional modeling. E_{fd} only saturates briefly following a disturbance.

by $a_2/\beta(\mathbf{x}_g)$, these oscillations produce swings with an approximate amplitude of 12 pu in E_{fd} which is more than sufficient to saturate E_{fd} at both limits [5].

VII. AVERAGING OF THE CONTROL INPUT

One way to mitigate the saturation problem is to subject the control input to a moving average. Mathematically, this means that the field voltage becomes

$$E_{fd} = \int_{t-T_0}^{t} \frac{\mathbf{a}^T\mathbf{z} - \rho(\mathbf{x}_g)}{\beta(\mathbf{x}_g)} d\tau. \tag{21}$$

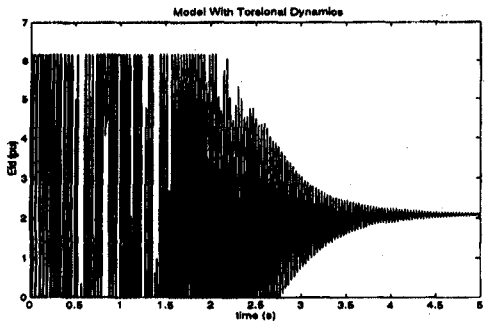

Fig. 7. Response of E_{fd} to a 0.5 s fault with torsional modeling. Clearly, the torsional dynamics cause E_{fd} to saturate for an extended period following the disturbance.

For this paper, the averaging is done over one period of the 60 Hz base frequency, so that $T_0 = 1/60$ s.

A. Linear Model of the System with Field Voltage Averaging

Averaging the feedback signal results in a nonlinear system. An approximate linear model can be developed, however, to represent the effects of filtering. First, recall that the original system has three low-frequency modes and four with frequencies in the torsional range. Recall that each mode in a linear system evolves independently. If the mode is not excited by initial conditions, then it will vanish for all time, regardless of the behavior of other modes. Our linear model of the system with control averaging will also consist of seven modes which act independently.

Second, notice that averaging is a low-pass operation. It is observed in simulations that the torsional oscillations are of significant amplitude only in the acceleration (z_3); therefore, we assume that all quantities in (21), except z_3, are unaffected by the averaging. The transfer function $H_a(j\omega)$ of the averaging process is

$$H_a(j\omega) = \frac{1}{j\omega}[1 - e^{-j\omega T_0}]. \tag{22}$$

Next, we observe that $z_3 = \alpha$ includes components from all seven modes. We approximate the averaging of α as the multiplication of each modal component of α by a constant which is equal to the transfer function of the integrator evaluated at the frequency of that mode. This approximation is reasonable since [6]

$$\alpha(t) = \sum_{i=1}^{n} \mathbf{w}_i^T \mathbf{x}(0) e^{\lambda_i t} [0\,0\,1\,0\,0\,0\,0] \mathbf{v}_i \tag{23}$$

where $\mathbf{w}$ and $\mathbf{v}$ are left and right eigenvectors, respectively, of the matrix $\mathbf{A}$. $\mathbf{A}$ is the seventh-order system matrix from (10). Using the notation

$$\lambda_i = \sigma_i + j\omega_i \tag{24}$$

we can write

$$\alpha_f(t) = \sum_{i=1}^{n} H_a(j\omega_i) \mathbf{w}_i^T \mathbf{x}(0) e^{\sigma_i t} [0\,0\,1\,0\,0\,0\,0] \mathbf{v}_i e^{j\omega_i t} \tag{25}$$

TABLE III
EIGENVALUES AND FREQUENCIES OF THE LINEAR MODEL OF AVERAGED FEEDBACK LINEARIZING CONTROL

Number(s)	Eigenvalue	Frequency (Hz)
1	-6.99	–
2,3	$-4.12 \pm j1.04$	0.1662
4,5	$0.19 \pm j198.92$	31.66
6,7	$-2.24 \pm j160.64$	25.57

where α_f is the averaged measurement of the acceleration. Notice in Table II that all eigenvalues have relatively small real parts; therefore, we treat $e^{\sigma_i t}$ as a constant. Note from (25) that the effect of the averaging of α is that the constant a_2 is replaced by $a_2 H_a(j\omega_i)$. We denote by $\mathbf{A}_{\omega_i}$ the matrix $\mathbf{A}$ with a_2 replaced by $a_2 H_a(j\omega_i)$.

Given the assumptions in this section, if an eigenvalue and eigenvector pair of frequency ω_i represents a mode of $\mathbf{A}_{\omega_i}$, then it must also be a mode of the averaged FBLC system, based on the following reasoning: If the initial condition $\mathbf{x}(0)$ of the averaged FBLC system is an eigenvector $\mathbf{v}_k$, then only mode k is excited, and $\dot{\mathbf{x}} = \mathbf{A}_{\omega_i}\mathbf{x}$ for all time. Mode k will evolve in the same fashion as if the system were linear with matrix $\mathbf{A}_{\omega_i}$. The modes are implicitly defined to act independently of each other. By finding the eigenvectors and eigenvalues of $\mathbf{A}_{\omega_i}$ for each modal frequency ω_i and picking out the modes that match those of the composite system, a matrix can be constructed to represent a linear model of the feedback-linearized system with field-voltage averaging.

The low frequency modes presented in Table II are presumed to be unaffected by the averaging and are incorporated directly into the linear model. An iterative scheme is used to find the remaining modes. We select an initial guess for ω_i from the eigenvalues of $\mathbf{A}$, the matrix for the nonaveraged system. Then we calculate $\mathbf{A}_{\omega_i}$, obtain a new value for ω_i from the eigenvalues of $\mathbf{A}_{\omega_i}$, and iterate until convergence. There is no proof that this algorithm actually does converge, but the frequencies are observed to experience only small shifts as ω_i changes, and for this example, three to six iterations are sufficient to provide an accurate estimate for ω_i. Finally, the eigenvalue of $\mathbf{A}_{\omega_i}$ that has imaginary part ω_i and its corresponding eigenvector are added to the linear model, along with their conjugates.

B. Results of Field Voltage Averaging

Calculation of the linear model with field-voltage averaging produces an unstable mode, as shown in Table III. This is confirmed by simulation, as shown in Fig. 8. The averaging introduces phase shifts of $-76.7°$ and $-95.0°$ at the torsional frequencies, and these phase shifts cause the instability. This will be examined further in the next section.

VIII. FILTERING OF THE ACCELERATION MEASUREMENT

Since control averaging leads to instability, we may attempt to remove the high-frequency content from the acceleration measurement with a low-pass filter. In this paper, Butterworth

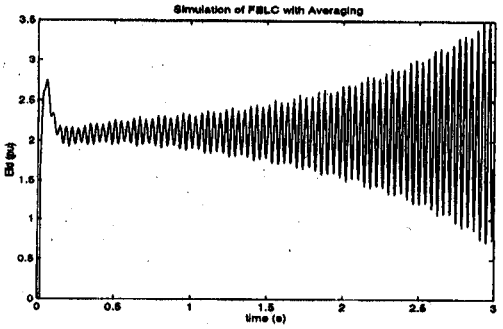

Fig. 8. Simulated response of E_{fd} to a small disturbance with averaged FBLC.

filters of several different orders are to perform the filtering. A Butterworth filter of order N has a transfer function $H_N(s)$ such that [10]

$$H_N(s)H_N(-s) = \frac{1}{1+(s/j\omega_c)^{2N}}. \tag{26}$$

A. Full Order Linear Model with Acceleration Filtering

The Butterworth filter connects with the system in such a way that the generator with torsional dynamics and acceleration filtering remains linear. The filter may be represented as a dynamic system with input α and output α_f. Only E_{fd} depends on the filtered acceleration measurement α_f; consequently, $\rho(\mathbf{x}_g)$ is a function of α_f, while $\rho_t(\mathbf{x}_g)$ is a function of the unfiltered acceleration α_e. The state equation for $\dot{\alpha}_e$ is

$$\dot{\alpha}_e = \frac{H}{H_e}(a_0(\delta_e-\delta_0)+a_1(\omega_e-\omega_o)+a_2\alpha_f) - \frac{\omega_o}{2H_e}\left[-K_{2eu}\frac{\omega_2}{\omega_o}+K_{2eu}\frac{\omega_e}{\omega_o}+D_{eu}\frac{\alpha_e}{\omega_o}-D\frac{\alpha_f}{\omega_o}\right]. \tag{27}$$

Combining this equation with the filter dynamics and feedback linearized generator/shaft model produces a linear model for the entire system.

B. Reduced Linear Model of Acceleration Filtering

The combination of the linear Butterworth filter and the feedback-linearized generator with torsional dynamics produces a composite system that remains linear. If the details of the filter are ignored and only the transfer function $H_N(j\omega)$ is considered at certain frequencies of interest, however, a seventh-order linear model of the system can be developed using the same reasoning that was employed when studying field voltage averaging, the only difference being that $H_N(j\omega)$ replaces $H_a(j\omega)$. The model developed in this fashion will be referred to as the reduced linear model, since the dynamics of the filter are ignored.

C. Results of Filtering the Acceleration Measurement

To examine the effects of measurement filtering, a first-, second-, and fourth-order Butterworth filter was used. In all cases, the cutoff frequency of the filter is 10 Hz which is at the low end of the range of shaft dynamics normally encountered. The eigenvalues of the reduced-order model and the full linear model for the three filter types are given in Tables IV–IX. The reduced-order model gives excellent agreement with the full-order model with respect to the torsional modes, but the low-frequency modes do not match up so well. This

TABLE IV
EIGENVALUES AND FREQUENCIES OF THE REDUCED LINEAR MODEL OF THE FEEDBACK LINEARIZING CONTROL WITH A FIRST-ORDER BUTTERWORTH FILTER OF ACCELERATION

Number(s)	Eigenvalue	Frequency (Hz)
1	-6.99	–
2,3	$-4.12 \pm j1.04$	0.1662
4,5	$-0.41 \pm j197.57$	31.44
6,7	$-1.85 \pm j155.96$	24.82

TABLE V
EIGENVALUES AND FREQUENCIES OF THE LINEAR MODEL OF FEEDBACK LINEARIZING CONTROL WITH A FIRST-ORDER BUTTERWORTH FILTER OF ACCELERATION

Number(s)	Eigenvalue	Frequency (Hz)
1	-17.36	–
2,3	$-3.18 \pm j1.38$	0.2197
4,5	$-0.41 \pm j197.57$	31.44
6,7	$-1.81 \pm j156.00$	24.83
8	-35.08	–

TABLE VI
EIGENVALUES AND FREQUENCIES OF THE REDUCED LINEAR MODEL OF FEEDBACK LINEARIZING CONTROL WITH A SECOND-ORDER BUTTERWORTH FILTER OF ACCELERATION

Number(s)	Eigenvalue	Frequency (Hz)
1	-6.99	–
2,3	$-4.12 \pm j1.04$	0.1662
4,5	$0.22 \pm j196.74$	31.31
6,7	$1.63 \pm j152.80$	24.32

TABLE VII
EIGENVALUES AND FREQUENCIES OF THE LINEAR MODEL OF FEEDBACK LINEARIZING CONTROL WITH A SECOND-ORDER BUTTERWORTH FILTER OF ACCELERATION

Number(s)	Eigenvalue	Frequency (Hz)
1	-21.07	–
2,3	$-3.02 \pm j1.41$	0.2247
4,5	$0.22 \pm j196.74$	31.31
6,7	$1.60 \pm j152.82$	24.32
8,9	$-32.88 \pm j31.23$	4.97

TABLE VIII
EIGENVALUES AND FREQUENCIES OF THE REDUCED LINEAR MODEL OF FEEDBACK LINEARIZING CONTROL WITH A FOURTH-ORDER BUTTERWORTH FILTER OF ACCELERATION

Number(s)	Eigenvalue	Frequency (Hz)
1	-6.99	-
2,3	$-4.12 \pm j1.04$	0.1662
4,5	$-0.09 \pm j196.59$	31.29
6,7	$-0.22 \pm j151.31$	24.08

TABLE IX
EIGENVALUES AND FREQUENCIES OF THE LINEAR MODEL OF FEEDBACK LINEARIZING CONTROL WITH A FOURTH-ORDER BUTTERWORTH FILTER OF ACCELERATION

Number(s)	Eigenvalue	Frequency (Hz)
1,2	$-0.09 \pm j196.59$	31.29
3,4	$-0.22 \pm j151.31$	24.08
5	-71.68	-
6,7	$-31.57 \pm j58.06$	9.24
8,9	$-2.70 \pm j1.44$	0.2287
10,11	$-11.87 \pm j22.89$	3.64

observation is best explained by noting that the real parts of the eigenvalues of the low frequency modes indicate that these modes decay fast enough to be affected by the filter.

Both the eigenvalues and the simulations indicate that the first- and fourth-order filters produce stable systems, while a second-order Butterworth filter results in an unstable system. The instability occurs because the second-order filter has a stopband phase shift of $-180°$ which inverts the high-frequency field voltage components and excites the torsional modes. Furthermore, the presence of any filter greatly reduces the damping of the torsional modes, approaching the natural damping in the shaft system. Eigenvalue analysis of the matrix $\mathbf{A}_\omega$ verifies these claims.

The fourth-order Butterworth filter significantly attenuates high-frequency components of the field voltage. Simulations of an FBLC-controlled system with fourth-order filtering of acceleration are shown in Figs. 9–11. The response of the rotor angle is almost identical to the simulation in Fig. 2, where torsional dynamics are not modeled. In this case, a fourth-order Butterworth filter results in improved performance of FBLC, but it must be cautioned that if any unmodeled dynamics exist near the cutoff frequency of the filter, they are very likely to be excited since the phase shift at the frequency is $-180°$ [5]. A more sophisticated filter design might be more robust in this respect.

IX. INCLUSION OF TORSIONAL DYNAMICS IN THE CONTROLLED DESIGN

Another approach to modifying FBLC in the presence of shaft dynamics is to change the control law to include them. Adding torsional state information to the controller, however,

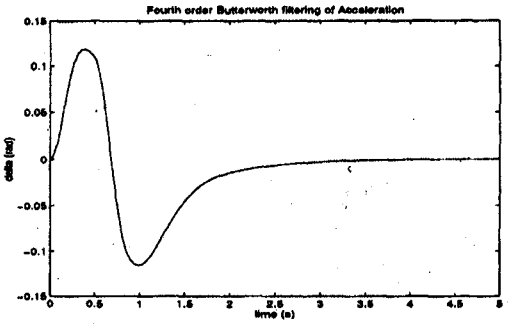

Fig. 9. Simulated response of $\delta - \delta_0$ to a 0.5 s fault with fourth-order Butterworth filtering of $\dot{\omega}$.

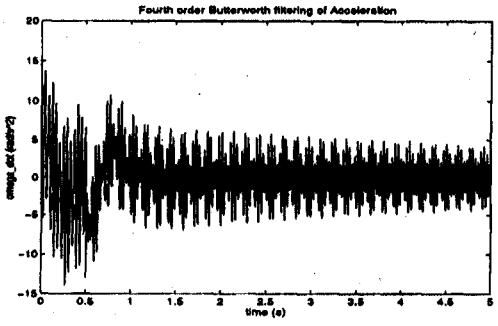

Fig. 10. Simulated response of $\dot{\omega}$ to a 0.5 s fault with fourth-order Butterworth filtering of $\dot{\omega}$.

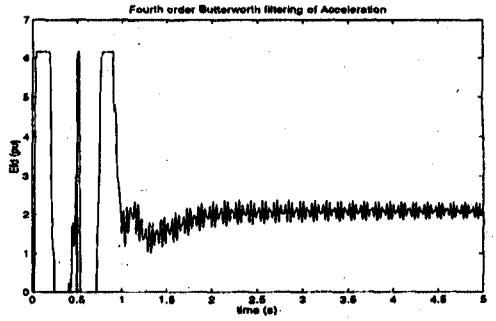

Fig. 11. Simulated response of E_{fd} to a 0.5 s fault with fourth-order Butterworth filtering of $\dot{\omega}$.

is not beneficial; in fact, because of field voltage saturation, the performance is seriously degraded. The shaft dynamics add enormous oscillations to $\rho_t(\mathbf{x}_g)$, and the given range of the field voltage is not nearly enough to control the system, as shown in Figs. 12–14 [5].

X. UNMODELED DYNAMICS OF THE TRANSMISSION SYSTEM

In addition to unmodeled dynamics of the device, we now include dynamics of the transmission elements that were previously neglected. The state vector of these system dynamics

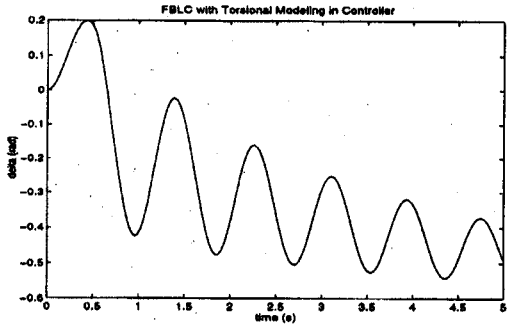

Fig. 12. Simulated response of $\delta - \delta_0$ to a 0.5 s fault with FBLC that accounts for torsional oscillations.

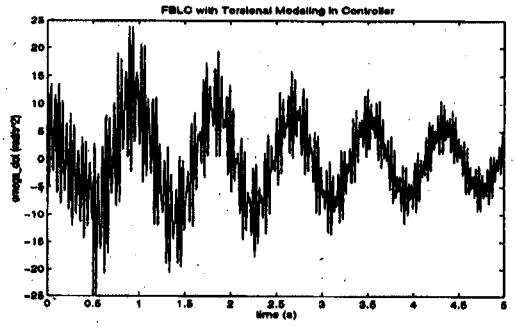

Fig. 13. Simulated response of $\dot{\omega}$ to a 0.5 s fault with FBLC that accounts for torsional oscillations.

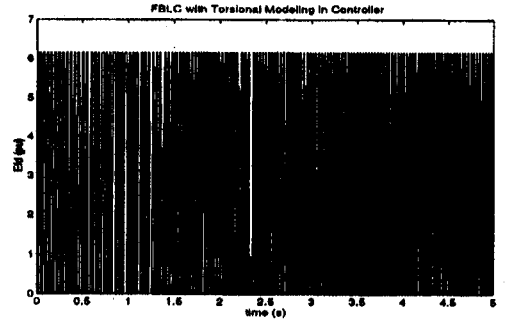

Fig. 14. Simulated response of E_{fd} to a 0.5 s fault with FBLC that accounts for torsional oscillations.

will be x_2 and the system equations become

$$\begin{bmatrix} \dot{z} \\ \dot{x}_1 \\ \dot{x}_2 \end{bmatrix} = f\left(\begin{bmatrix} z \\ x_1 \\ x_2 \end{bmatrix} \right). \tag{28}$$

Note that we no longer assume linearity of the complete system. To perform eigenvalue analysis, we linearize (28) around the equilibrium point. If a more conventional linear controller is used, the linearized closed-loop dynamics are of the form

$$\begin{bmatrix} \dot{\Delta z} \\ \dot{\Delta x}_1 \\ \dot{\Delta x}_2 \end{bmatrix} = \begin{bmatrix} A_{11} & A_{12} & A_{13} \\ A_{21} & A_{22} & A_{23} \\ A_{31} & A_{32} & A_{33} \end{bmatrix} \begin{bmatrix} \Delta z \\ \Delta x_1 \\ \Delta x_2 \end{bmatrix} \tag{29}$$

where the Δ indicates a small deviation of a state vector from equilibrium.

On the other hand, if exact FBLC is employed, the linearized closed-loop dynamics of the complete system are of a (partially) decoupled form

$$\begin{bmatrix} \dot{\Delta z} \\ \dot{\Delta x}_1 \\ \dot{\Delta x}_2 \end{bmatrix} = \begin{bmatrix} A_{11} & A_{12} & 0 \\ A_{21} & A_{22} & 0 \\ A_{31} & A_{32} & A_{33} \end{bmatrix} \begin{bmatrix} \Delta z \\ \Delta x_1 \\ \Delta x_2 \end{bmatrix}. \tag{30}$$

We begin to have potential instabilities in (29) in modes which respond to both x_1 and x_2. If the control input is not constrained, however, no instabilities occur in (30). The effects of saturation limit the stabilizing ability of FBLC; however, in most practical tests with saturation, FBLC was still able to prevent instability from developing.

XI. Effects of Feedback Linearizing Control on Subsynchronous Resonance

We saw earlier that feedback linearizing control increases the damping of the shaft modes. We now wish to investigate the effect that increased damping has on subsynchronous resonance, since the torsional dynamics play a pivotal role in this phenomenon.

A. Model of the Network

To analyze subsynchronous resonance, it is necessary to develop a model for the network dynamics to be added to the generator and shaft models in Sections IV and V. Following [11], the following time-varying phasor model is used to capture the electromagnetic dynamics of the transmission grid:

$$\hat{V}_R = \hat{Z}_R \hat{I}_R \tag{31}$$

$$\hat{V}_L = L\frac{d\hat{I}_L}{dt} + \hat{Z}_L \hat{I}_L \tag{32}$$

$$\hat{I}_C = C\frac{d\hat{V}_C}{dt} + \hat{Y}_C \hat{V}_C. \tag{33}$$

Normally, the voltage and current phasors are assumed to vary slowly with time, so the time derivatives are ignored. Subsynchronous currents appear in phasor notation with a time-varying component, however. For example, time domain and phasor representations of a 30 Hz subsynchronous current take the following forms:

$$i(t) = 5\cos 60\pi t \leftrightarrow \hat{I} = 5e^{-j60\pi t} \tag{34}$$

since $i(t) = \mathcal{R}(\hat{I}e^{j\omega_o t})$, where $\omega_o = 120\pi$. Therefore, the time derivatives in (32) and (33) cannot be neglected.

The network we consider is shown in Fig. 15. It consists of a generator, a transmission line, a series capacitor, and an infinite bus. The transmission line resistance and reactance includes generator resistance and transient reactance, so that the states

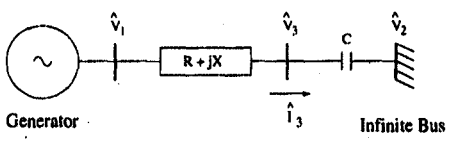

Fig. 15. Network for subsynchronous resonance simulation.

E'_d and E'_q can be treated as the voltage at the generator bus after an appropriate coordinate transform. The voltage and current at bus 3 (the connection between the transmission line and the series capacitor) will be the state variables for the network. Note that we neglect shunt capacitance. The current is therefore the same throughout the network.

Since the current through the transmission line inductance is simply $\hat{I}_3$, we may write

$$\hat{V}_1 - \hat{V}_3 = \frac{X}{\omega_o}\frac{d\hat{I}_3}{dt} + (R + jX)\hat{I}_3. \tag{35}$$

The capacitor voltage is equal to $\hat{V}_3 - \hat{V}_2$, where $\hat{V}_2 = W_d + jW_q$ represents the infinite bus voltage. This leads to the following equation:

$$\hat{I}_3 = C\frac{d\hat{V}_3}{dt} + j\omega_o C(\hat{V}_3 - W_d - jW_q). \tag{36}$$

Equations (35) and (36) can be used to define two complex-valued or four real-valued states. Denoting $\hat{I}_3 = I_{d3} + jI_{q3}$ and $\hat{V}_3 = V_{d3} + jV_{q3}$, we have the following state equations for a single transmission line with capacitive compensation:

$$\dot{I}_{d3} = \frac{\omega_o}{X}[V_{d1} - V_{d3} - RI_{d3} + XI_{q3}] \tag{37}$$

$$\dot{I}_{q3} = \frac{\omega_o}{X}[V_{q1} - V_{q3} - RI_{q3} + XI_{d3}] \tag{38}$$

$$\dot{V}_{d3} = \frac{1}{C}I_{d3} + \omega_o(V_{q3} - W_q) \tag{39}$$

$$\dot{V}_{q3} = \frac{1}{C}I_{q3} + \omega_o(V_{d3} - W_d). \tag{40}$$

B. Sample Network Parameters

As before, parameter values from typical examples are selected to perform simulations of the system. For the transmission line, $R = 0.058526$ and $X = 0.89497$; this corresponds to the admittance used in earlier simulations. $\hat{V}_2$, the infinite bus voltage, was chosen so that $\hat{V}_3$ maintained an equilibrium value of $0.9164 + j0.20473$, regardless of the capacitance selected; this was done so that the system would maintain the same equilibrium point for a variety of capacitor values. With these network constraints, the generator maintains the same equilibrium as in previous simulations.

C. Simulation Results

Once the models are determined, simulations are straightforward. A slight perturbation of the line current was used as a disturbance.

First, a constant excitation voltage was used to demonstrate the natural dynamics of the system. The simulator includes a routine to numerically derive a linearized state-space representation of a system at any given operating point.

TABLE X
EIGENVALUES AND FREQUENCIES OF THE LINEARIZED SYSTEM FOR THREE EXAMPLE SERIES CAPACITOR VALUES

Compensation	Eigenvalue	Frequency (Hz)
2.96%	$-9.90 \pm j441.1$	70.20
	$-8.95 \pm j312.6$	49.75
	$-0.058 \pm j196.6$	31.29
	$-0.051 \pm j151.6$	24.13
	-34.84	-
	-30.90	-
	$-0.459 \pm j6.71$	1.07
	-4.88	
	-0.328	-
23.0%	$-10.41 \pm j557.4$	88.71
	$-7.95 \pm j196.1$	31.21
	$0.808 \pm j196.5$	31.27
	$0.061 \pm j152.2$	24.22
	-35.87	-
	-32.25	-
	$-0.644 \pm j7.65$	1.22
	-0.356	-
	-5.03	-
35.9%	$-10.55 \pm j602.7$	95.92
	$-0.053 \pm j196.4$	31.26
	$-9.35 \pm j151.7$	24.15
	$3.85 \pm j151.5$	24.11
	-36.79	-
	-33.60	-
	$-0.832 \pm j8.40$	1.34
	-0.378	-
	-5.14	-

The resulting eigenvalues of the linearized model for three selected capacitance values are shown in Table X. With a large capacitor in series with the transmission line, the system remains stable. At 23.0% compensation, however, the subsynchronous frequency drops to about 31.3 Hz and interacts with a torsional mode at that frequency, causing instability. At 35.9% compensation, the subsynchronous currents interact with the torsional mode at 24 Hz, again leading to instability. A simulation of the system with 23.0% compensation is shown in Fig. 16, illustrating the unstable subsynchronous oscillations.

Next, the effect of FBLC on a system prone to subsynchronous resonance is examined. The results of a test run with FBLC poles at -5 and 23.0% series compensation are shown in Figs. 17 and 18. Even though the series capacitance is at a critical value, FBLC does stabilize the system. Note that the field voltage reacts at a high frequency during the transient. Although these results seem quite surprising, the placement of the poles at -5 causes the generator to act as a low pass filter and damp out high-frequency mechanical components which would otherwise interact with the magnetic fields produced in the air gap by subsynchronous currents. The large, fast swings in E_{fd} shown in Fig. 18 are generally undesirable. To reduce these swings, a fourth-order Butterworth filter was added to the acceleration measurement to reduce the swings while still

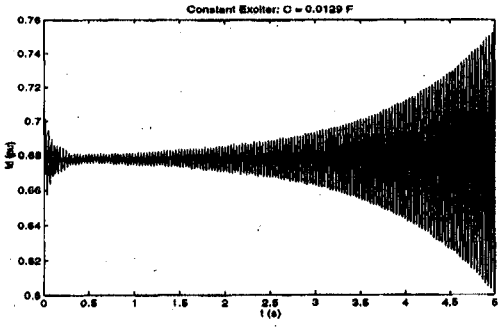

Fig. 16. Line current (real part of phasor) of a system experiencing subsynchronous resonance.

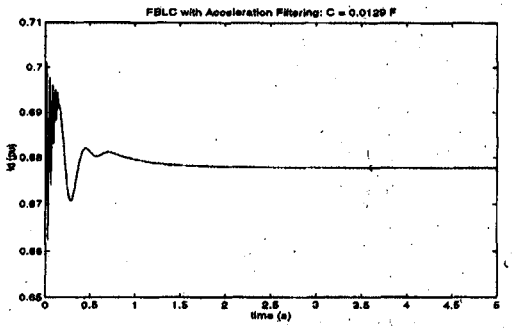

Fig. 19. Line current (real part of phasor) of a system with 23.0% compensation and FBLC with fourth-order Butterworth acceleration filtering.

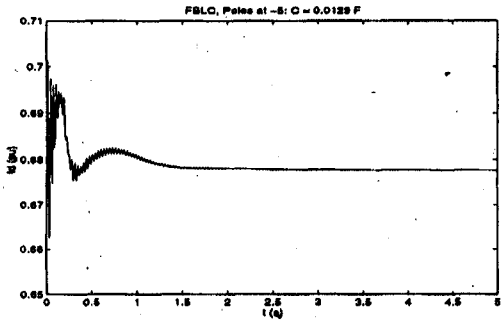

Fig. 17. Line current (real part of phasor) of a system with 23.0% compensation and FBLC.

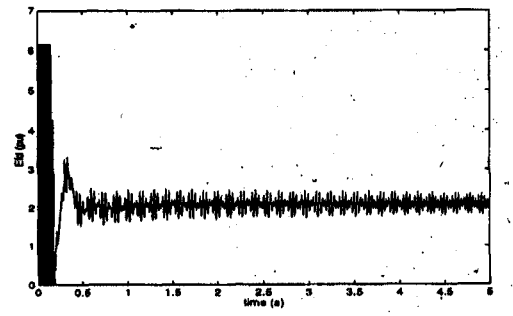

Fig. 20. Field voltage of a system with 23.0% compensation and FBLC with fourth-order Butterworth acceleration filtering.

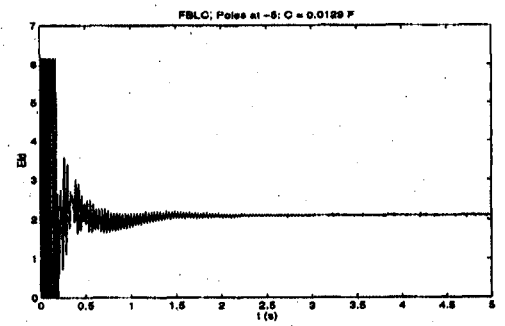

Fig. 18. Field voltage of a system with 23.0% compensation and FBLC.

providing the control necessary to stabilize the system. The results of the acceleration filtering method with poles placed at -5 are shown in Figs. 19 and 20. These results are very surprising, since we might expect that the high frequency oscillations in the field voltage are too small to stabilize the subsynchronous modes. The simulations reveal, however, that the torsional modes do not grow.

XII. Robust Stability of a System

Robust stability with respect to parametric uncertainty of the shaft model will be defined and analyzed in terms of the roots of the uncertain polynomial

$$p(s, \mathbf{q}) = a_n(\mathbf{q})s^n + a_{n-1}(\mathbf{q})s^{n-1} + \cdots + a_1(\mathbf{q})s + a_0(\mathbf{q}) \tag{41}$$

where the coefficients $a_i(\mathbf{q})$ are real functions of uncertain quantities $\mathbf{q} = [q_1\ q_2 \ldots q_m]^T$ and $q_i^- \le q_i \le q_i^+$. The polynomial $p(s, \mathbf{q})$ is robustly stable if and only if all roots of $p(s, \mathbf{q}) = 0$ are in the left half plane for all $\mathbf{q} \in Q$, where Q denotes the set of all possible uncertainty vectors $\mathbf{q}$. The polynomial we will be analyzing is the characteristic polynomial of the system in (10)

$$p(s, \mathbf{q}) = \det\left(s\mathbf{I} - \begin{bmatrix} \mathbf{A}_{11} & \mathbf{A}_{12} \\ \mathbf{A}_{21} & \mathbf{A}_{22} \end{bmatrix}\right). \tag{42}$$

Throughout this paper, it is assumed that $a_n(\mathbf{q}) \neq 0$ for all $\mathbf{q} \in Q$. This condition is equivalent to stating that $p(s, \mathbf{q})$ has invariant degree, meaning that the number of roots is the same for all $\mathbf{q}$. It can be shown that (42) has invariant degree.

The manner in which the uncertain quantities q_i appear in the polynomial coefficients is known as the uncertainty structure. If each q_i appears in only one coefficient, the polynomial has an independent uncertainty structure. If at least one q_i appears in more than one coefficient, but every term of every coefficient has at most one uncertain quantity, the uncertainty structure is affine linear. If there are terms which

contain products of different q_i, but there are no powers of any q_i greater than one, the structure is multilinear. An uncertainty structure with higher powers of at least one q_i is polynomic. The uncertainty structure for the torsional shaft/generator system with FBLC is a multilinear structure.

A. Kharitonov's Theorem

Perhaps the most well known and simplest tool for robust stability analysis is Kharitonov's Theorem. Kharitonov's Theorem is a conclusive test for the stability of an independent uncertainty structure. Such a polynomial may be written as

$$p(s, \mathbf{q}) = q_n s^n + q_{n-1} s^{n-1} + \cdots + q_1 s + q_0 \qquad (43)$$

where, as before, $q_i^- \leq q_i \leq q_i^+$. Kharitonov's theorem asserts that $p(s, \mathbf{q}) = 0$ is robustly stable if and only if the four Kharitonov polynomials are stable [12].

This theorem provides a simple, conclusive test for robust stability. By calculating the roots of four polynomials, we have information about an entire set of polynomials. It is well known, however, that the required independent uncertainty structure rarely occurs in practice. It is possible to apply Kharitonov's Theorem to any uncertainty structure by finding the uncertainty range of each coefficient; this technique is called overbounding [12]. Since the coefficients are not free to vary independently, however, the results of overbounding are conservative. If Kharitonov's Theorem concludes stability for the overbounded structure, then the original structure is robustly stable; however, the converse is not true. If the test fails, other techniques are required to determine whether the system is robustly stable.

B. Value Set and the Zero Exclusion Condition

For any generalized uncertainty structure, robust stability may be determined by means of the value set. The value set at a given frequency ω_o is defined as the region covered by $p(j\omega_o, \mathbf{q})$ for all $\mathbf{q} \in Q$. For specialized uncertainty structures, the value set has a distinct shape which will be discussed later [12].

The value set is used to conclusively determine robust stability of $p(s, \mathbf{q})$ through the Zero Exclusion Condition. This condition states that $p(s, \mathbf{q})$ is robustly stable if and only if at least one member of $p(s, \mathbf{q})$ is stable, and the value set $p(j\omega, \mathbf{q})$ does not include the point zero at any frequency ω, where $0 \leq \omega \leq \infty$. The proof of the Zero Exclusion Condition is based on the following argument: If $p(s, \mathbf{q})$ is robustly stable, then the roots of $p(s, \mathbf{q}) = 0$ must always be in the left half plane, and $p(j\omega, \mathbf{q})$ can never be zero, since $j\omega$ is on the imaginary axis. Furthermore, if $p(s, \mathbf{q})$ is not robustly stable, then for some $\mathbf{q}_s \in Q$ and $\mathbf{q}_u \in Q$, $p(s, \mathbf{q}_s)$ is stable while $p(s, \mathbf{q}_u)$ is not. As $\mathbf{q}$ travels on a path from $\mathbf{q}_s$ to $\mathbf{q}_u$, at least one root of $p(s, \mathbf{q})$ travels from the left half plane to the right half plane; for some $\mathbf{q}^*$ on the path, that root crosses the imaginary axis at $j\omega^*$, and therefore $p(j\omega^*, \mathbf{q}^*) = 0$. Note that because the coefficients of $p(s, \mathbf{q})$ are assumed to be real, it is sufficient to check the positive imaginary axis, since imaginary roots occur in conjugate pairs. A formal proof may be found in [12].

C. The Structure of the Value Set

To apply to Zero Exclusion Condition, the boundaries of the value set for the full range of ω must be known or approximate. The Zero Exclusion Condition is the basis for the proof of Kharitonov's Theorem which applies to the independent uncertainty structure. The value set for an independent uncertainty structure is a rectangle. To see this, note from (43)

$$p(j\omega_0, \mathbf{q}) = (q_0 - q_2\omega_o^2 + q_4\omega_o^4 - \cdots) + j(q_1\omega_o - q_3\omega_o^3 + \cdots). \qquad (44)$$

Because of the independence of the coefficients, the real and imaginary parts of the polynomial may be maximized independently, hence the shape of the values set is a rectangle for any ω. It can be shown that the Zero Exclusion Condition for the Kharitonov rectangle is satisfied if and only if the four Kharitonov polynomials are stable [12].

If the uncertainty structure is affine linear, the value set will be a convex polygon. For multilinear uncertainty structures, the value set no longer has a well-defined shape. An upper bound for the value set of a multilinear structure may be determined, however, using the Mapping Theorem [12]. First, it is necessary to calculate $p(j\omega, \mathbf{q})$ for all of the extrema of $\mathbf{q}$. The extrema are the points where each q_i is at either its minimum or maximum value. Notice that Q has the shape of a box; the extrema correspond to the corners of the box. Furthermore, the number of extrema is equal to 2^m, where m is the number of uncertainties.

Next, the value set $p(j\omega, \mathbf{q})$ is included within the convex hull of the extrema. The convex hull of a set is the intersection of all convex sets containing it. If the uncertainty structure is affine linear, then the convex hull of the extrema is the value set.

XIII. Analyzing the Torsional Shaft/Generator System

We are now prepared to apply the Zero Exclusion Condition to analyze the stability robustness of the shaft/generator system. Since the coefficients a_i are always negative (it is clearly undesirable to place the FBLC closed-loop poles in the right half plane), all of the terms in each coefficient of the characteristic polynomial are positive [5]. This simplifies the task of bounding the coefficient uncertainty, but the multilinear uncertainty structure makes the calculation of the value set difficult, and it is therefore not possible to conclusively establish robust stability over a wide variation of many system parameters without an exorbitant amount of computation.

A. Damping Parameters

We first examine the system stability when the spring coefficients are fixed and the damping coefficients vary over a wide range. Assume that the per unit damping terms lie

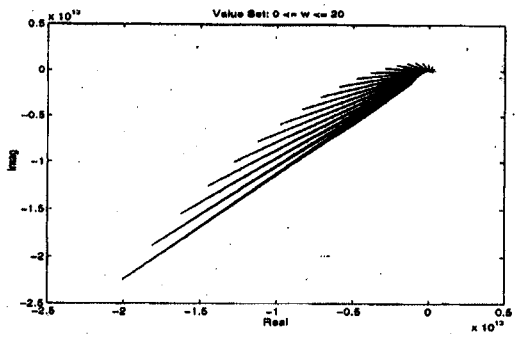

Fig. 21. Value set for $0 \leq \omega \leq 20$.

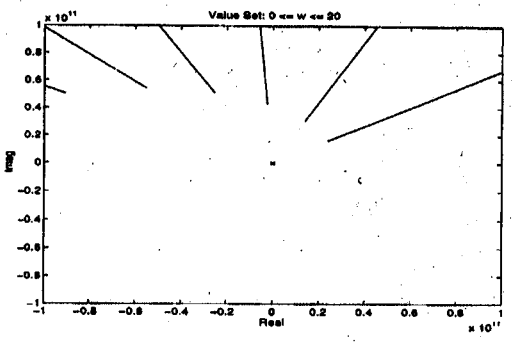

Fig. 22. Value set for $0 \leq \omega \leq 20$.

within the following ranges:

$$0 \leq D_{1u} \leq 0.32$$
$$0 \leq D_{2u} \leq 2$$
$$0 \leq D_{eu} \leq 1.2$$

while the other parameters are fixed. Overbounding with Kharitonov's Theorem is sufficient to establish that the system is robustly stable within these bounds. It is easily verified that the roots of the four Kharitonov polynomials are all in the left half plane [5].

B. Spring Constant Parameters

Next, we allow a large variation in the spring constants K_{12u} and K_{2eu}, while fixing the remaining parameters. We set the uncertainty bounds for the spring constants as

$$10^4 \leq K_{12u} \leq 4 \times 10^4$$
$$2 \times 10^4 \leq K_{2eu} \leq 8 \times 10^4.$$

Unfortunately, overbounding is too conservative in this case, making it necessary to resort to calculation of the value set for $0 \leq \omega \leq 1000$. Note that it is not necessary to generate an infinite number of value sets in order to verify the Zero Exclusion Condition, since the highest-order term of the characteristic polynomial eventually dominates, assuring that zero is not included in the value set above a certain frequency.

The value sets for $0 \leq \omega \leq 1000$ are shown in Figs. 21–27. For $135 \leq \omega \leq 265$, the convex hull of the extreme points does include the zero point. To show that the value set at these frequencies does not include zero, two convex hulls are generated: one for $10^4 \leq K_{12u} \leq (\omega/131)^2 \times 10^4$ and another for $(\omega/131)^2 \times 10^4 \leq K_{12u} \leq 4 \times 10^4$. The value set $p(j\omega, \mathbf{q})$ is contained in the union of the two smaller convex hulls. Since the value set does not include zero at any frequency, we conclude that the system is robustly stable to the specified parameter variations in the spring constants.

XIV. Sliding Control

Referring to (3) and (6), uncertainties in the shaft model produce uncertainties in $\rho(\mathbf{x}_g)$ and $\beta(\mathbf{x}_g)$, and hence a control methodology that accounts in some way for these uncertainties might be more appropriate. One such method is known as

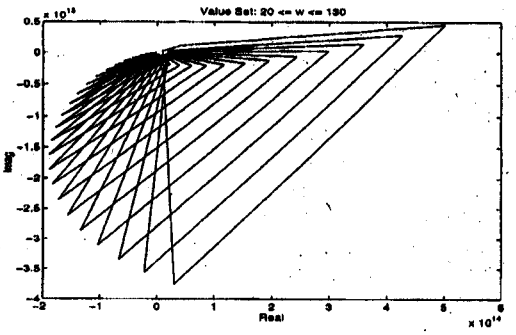

Fig. 23. Value set for $20 \leq \omega \leq 130$.

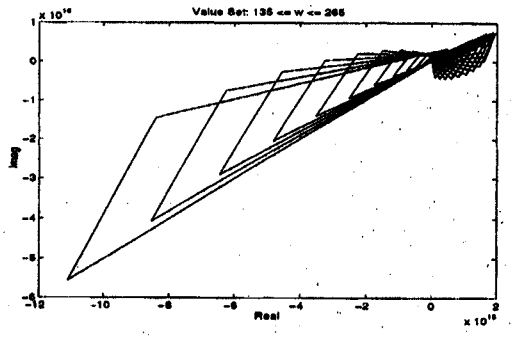

Fig. 24. Value set for $135 \leq \omega \leq 265$.

sliding control [13]. In a sliding control design, the system states are designed to follow a desired trajectory despite inaccuracies in the model. We choose the desired trajectory to reflect the response of a linear system. The control is designed so that $\mathbf{z}(t)$ will follow a specified trajectory, denoted as $\mathbf{z}^*(t)$. The tracking error is then

$$\tilde{\mathbf{z}} = \mathbf{z} - \mathbf{z}^*. \tag{45}$$

A. The Sliding Surface

Sliding control gets its name because the system states are constrained by the control to "slide" along an $n-1$-dimensional surface. The surface is defined by the constraint

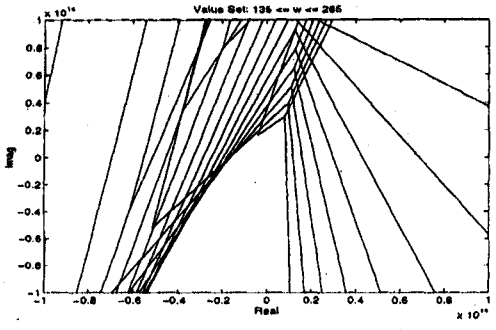

Fig. 25. Value set for $135 \leq \omega \leq 265$.

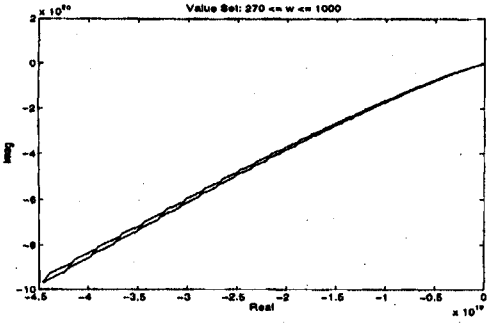

Fig. 26. Value set for $270 \leq \omega \leq 1000$.

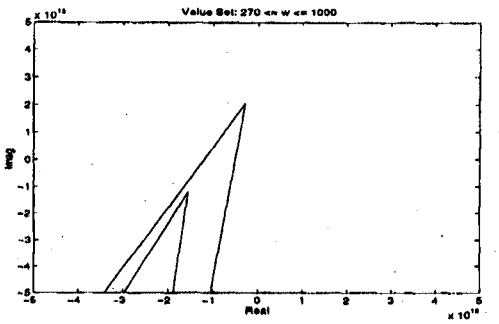

Fig. 27. Value set for $270 \leq \omega \leq 1000$.

$s(\mathbf{z}, t) = 0$, where [13]

$$s(\mathbf{z}, t) = \left(\frac{d}{dt} + \lambda\right)^{n-1} \tilde{z}_1 \tag{46}$$

where λ is a positive constant and n is the order of the system. In the present case, $n = 3$, and therefore

$$s(\mathbf{z}, t) = \ddot{\tilde{z}}_1 + 2\lambda\dot{\tilde{z}}_1 + \lambda^2\tilde{z}_1 \tag{47}$$

which may be written as

$$s(\mathbf{z}, t) = \tilde{z}_3 + 2\lambda\tilde{z}_2 + \lambda^2\tilde{z}_1. \tag{48}$$

If the initial state is such that

$$\mathbf{z}(0) = \mathbf{z}^*(0) \tag{49}$$

then the tracking problem $\mathbf{z}(t) = \mathbf{z}^*(t)$ or $\tilde{\mathbf{z}} = 0$ is equivalent to $s(\mathbf{z}, t) = 0$. This means that perfect tracking is achieved if (49) is satisfied and $\mathbf{z}(t)$ remains exactly on the surface for all time. If $\mathbf{z}(0) \neq \mathbf{z}^*(0)$, but $s(\mathbf{z}, t) = 0$, then s forms a differential equation in $\tilde{z}_1$ whose solution consists of decaying exponentials. This means that if $\mathbf{z}(t)$ is on the surface for all time, $\mathbf{z}(t)$ approaches $\mathbf{z}^*(t)$ exponentially with a time constant of $(n-1)/\lambda$. When z is on the surface, the system is said to be in sliding mode. The key of sliding control is that a first-order problem in s replaces an nth-order vector problem [13].

We therefore desire that $s = 0$ for all time. This constraint will be achieved if the control input u is selected so that, for $s \neq 0$ and a positive constant η

$$\frac{1}{2}\frac{d}{dt}s^2 \leq -\eta|s|. \tag{50}$$

This condition means that all system trajectories that are off of the surface must travel toward the surface. The time to reach the surface will be less than $s(t = 0)/\eta$ [13]. Furthermore, (50) guarantees that $\mathbf{z}(t)$ will reach the surface in a finite time, if $\mathbf{z}(0)$ is not on the surface.

B. Choosing a Control Input

We can formulate a control law for the sliding controller by differentiating s with respect to time

$$\dot{s} = \dot{\tilde{z}}_3 + 2\lambda\dot{\tilde{z}}_2 + \lambda^2\dot{\tilde{z}}_1. \tag{51}$$

Substituting for the derivatives and setting $\dot{s} = 0$

$$\rho(\mathbf{z}) + \beta(\mathbf{z})u - \dot{z}_3^* + 2\lambda\tilde{z}_3 + \lambda^2\tilde{z}_2 = 0 \tag{52}$$

where $\rho(\mathbf{z})$ and $\beta(\mathbf{z})$ represent the estimated values of these quantities that are used by the controller. Solving for $u = u_e$ gives the nominal control input

$$u_e = \frac{-\rho(\mathbf{z}) + \dot{z}_3^* - 2\lambda\tilde{z}_3 - \lambda^2\tilde{z}_2}{\beta(\mathbf{z})}. \tag{53}$$

To ensure that u satisfies (50) despite the presence of uncertainties in $\rho(\mathbf{z})$ and $\beta(\mathbf{z})$, an extra term is added to the control input

$$u = \frac{-\rho(\mathbf{z}) + \dot{z}_3^* - 2\lambda\tilde{z}_3 - \lambda^2\tilde{z}_2 - k\,\mathrm{sgn}\,(s)}{\beta(\mathbf{z})} \tag{54}$$

$\mathrm{sgn}(s)$ is the sign function, defined as

$$\mathrm{sgn}\,(s) = \begin{array}{ll} 1 & s > 0 \\ -1 & s < 0. \end{array} \tag{55}$$

If the error $|\rho(\mathbf{z}) - \rho_t(\mathbf{z})| \leq F$ and $B^{-1} \leq \beta(\mathbf{z})/\beta_t(\mathbf{z}) \leq B$, then the control input will satisfy (50) if

$$k \geq B(F + \eta) + (B - 1)|u_e|. \tag{56}$$

The implementation of (54) as a control law results in a system that tracks the desired trajectory very closely. Note, however, that the control input in (54) is discontinuous across the surface. Consequently, because switching does not occur at an infinite speed, the control will chatter as s rapidly oscillates around zero [13]. In the next section, we will see how to prevent chattering while still maintaining good performance.

C. The Boundary Layer

To prevent chattering, it is necessary to remove the constraint that s be perfectly zero; instead we will constrain $|s| \leq \Phi$. Consequently, this means that instead of trying to remain exactly on the surface, we will remain near the surface within a boundary layer of thickness Φ. It can be shown that if $\mathbf{z}(0) = \mathbf{z}^*(0)$ and $|s| \leq \Phi$ for all time, then the tracking error will be limited such that [13]

$$|\tilde{z}_i(t)| \leq (2\lambda)^i \frac{\Phi}{\lambda^{n-1}}. \tag{57}$$

If $\mathbf{z}(0) \neq \mathbf{z}^*(0)$, then this bound is approached exponentially with a time constant of $(n-1)/\lambda$ if $|s| \leq \Phi$ for all time.

Outside of the boundary layer, the control law for u is the same as before. To achieve a boundary layer, we simply change the control law to

$$u = \frac{-\rho(\mathbf{z}) + \dot{z}_3^* - 2\lambda\dot{\tilde{z}}_2 - \lambda^2\dot{\tilde{z}}_1 - k\,\mathrm{sat}\,(s/\Phi)}{\beta(\mathbf{z})} \tag{58}$$

$\mathrm{sat}(s)$ is the saturation function, defined as

$$\mathrm{sat}(s) = \begin{array}{ll} 1 & s > 1 \\ -1 & s < -1 \\ s & -1 \leq s \leq 1. \end{array} \tag{59}$$

Since (50) is still satisfied for all points outside the boundary layer, all trajectories must point towards the layer. We will treat the boundary layer thickness Φ as constant, although it can be allowed to vary with time [13].

D. Selection of Controller Parameters

The sliding mode controller design includes several parameters. The parameter λ is referred to as the control bandwidth. As shown by (57), a larger λ results in less tracking error, even if large modeling errors are present. The maximum allowable λ is limited however, by the presence of high frequency unmodeled dynamics and time delays.

The parameter η represents the time required for the states to reach the surface. Note from (56) that increasing k results in an increase in η, reducing the reaching time. A larger k increases the tendency and magnitude of control chattering, however, which means that a larger Φ will be needed; consequently, the tracking error on the surface will be larger. The boundary layer thickness Φ is generally chosen to be as small as possible while still preventing control chattering [13].

E. Sliding Mode Controller Design for a Generator

We are now ready to design a sliding control design for the third-order generator model. Because the field voltage can not vary infinitely, the following design is actually a hybrid FBLC/sliding control scheme. First, we choose the desired trajectory to be the response of the following linear system:

$$\mathbf{z}^* = \mathbf{A}\mathbf{z}^* \tag{60}$$

$$\mathbf{A} = \begin{bmatrix} 0 & 1 & 0 \\ 0 & 0 & 1 \\ a_0 & a_1 & a_2 \end{bmatrix}.$$

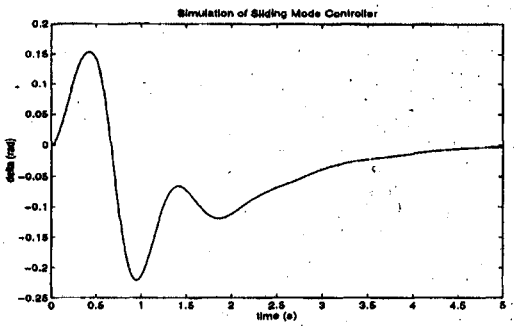

Fig. 28. Response of $\delta - \delta_o$ to a 0.5 s fault with sliding control.

This is the same system that we were trying to create using FBLC. The trajectory may therefore be written as the following time function:

$$\mathbf{z}^*(t) = e^{\mathbf{A}t}\mathbf{z}(0) \tag{61}$$

where we have chosen $\mathbf{z}^*(0) = \mathbf{z}(0)$ so that the control always operates on the surface. Although the calculation of the trajectory seems to be a formidable task, the appropriate time functions are the solutions of the differential equation

$$z_1^{*(3)} - a_2\ddot{z}_1^* - a_1\dot{z}_1^* - a_0 z_1^* = 0. \tag{62}$$

The controller parameters were selected as $\lambda = 5$, $k = 1$, and $\Phi = 0.25$.

To handle field voltage saturation, the following algorithm was used. Initially, $\mathbf{z}^* = 0$, so that the desired trajectory is at equilibrium and constant for all time. The controller is implemented as a discrete-time system with sampling frequency of 100 Hz. At each time step, the controller calculates a new value of E_{fd} using the sliding control laws. If E_{fd} saturates at either limit, then at the next time step, the value of E_{fd} is calculated by the FBLC control law, i.e.,

$$E_{fd} = \frac{\mathbf{a}^T\mathbf{z} - \rho(\mathbf{z})}{\beta(\mathbf{z})}. \tag{63}$$

As long as the value of E_{fd} remains saturated, the FBLC control law is applied. When E_{fd} comes out of saturation, the state vector $\mathbf{z}$ at that time step becomes the initial state of the desired trajectory, and sliding control is again applied to the system. Sliding control is maintained as long as E_{fd} does not saturate. In this algorithm, FBLC is used to monitor the field voltage and determine when to restart sliding mode control [5].

F. Simulations of a Sliding Mode Control

To examine the effects of torsional dynamics on a sliding mode controller, numerical simulations are performed. The controller is tested by simulating the same 0.5 s fault that was used in earlier simulations. Plots of the simulation results are shown in Figs. 28–34. According to the simulations, the response of sliding mode control to torsional oscillations is virtually the same as that of FBLC. The uncertainty in $\rho_t(\mathbf{x}_g)$ because of torsional oscillations is clearly very large, although because the oscillations are at a high frequency, it

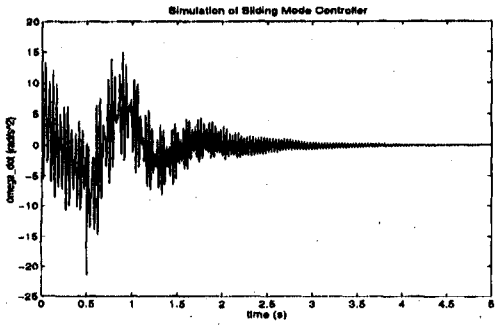

Fig. 29. Response of $\dot{\omega}$ to a 0.5 s fault with sliding control.

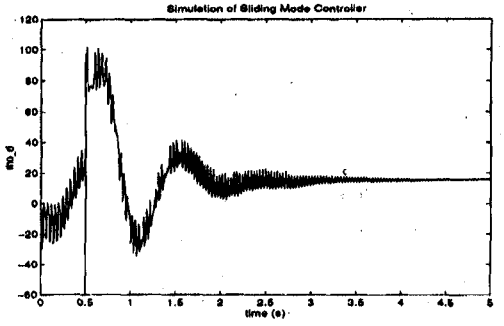

Fig. 32. Response of $\rho(\mathbf{x}_g)$ to a 0.5 s fault with sliding control.

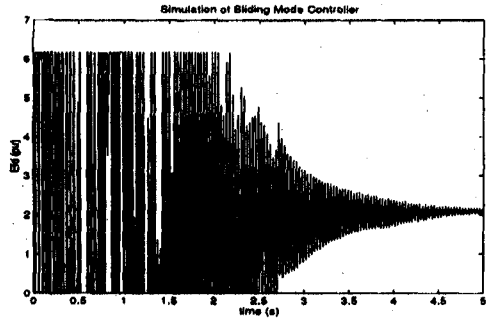

Fig. 30. Response of E_{fd} to a 0.5 s fault with sliding control.

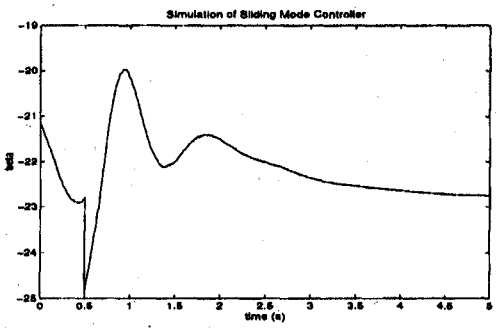

Fig. 33. Response of $\beta_t(\mathbf{x}_g)$ to a 0.5 s fault with sliding control.

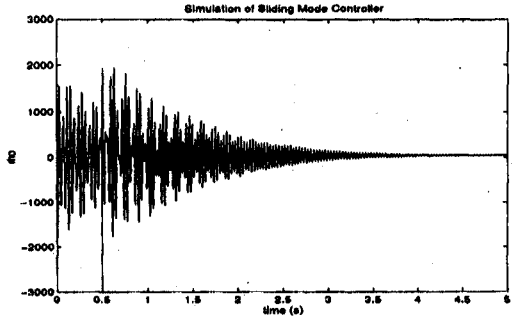

Fig. 31. Response of $\rho_t(\mathbf{x}_g)$ to a 0.5 s fault with sliding control.

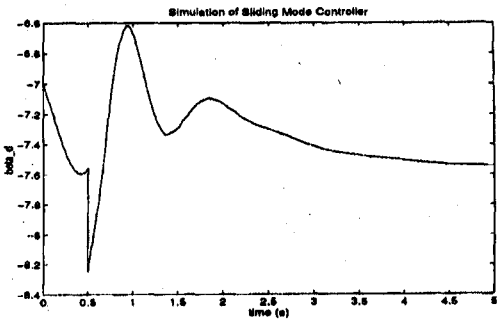

Fig. 34. Response of $\beta(\mathbf{x}_g)$ to a 0.5 s fault with sliding control.

appears that they are averaged out by the controller and the resulting performance is no different from FBLC. A plot of $\omega_e - \omega_2$ is given in Fig. 35; since $\rho_t(\mathbf{x}_g)$ includes the quantity $K_{2eu}(\omega_e - \omega_2)$, where K_{2eu} is on the order of 10^4, the spring constant terms dominate the quantity $\rho_t(\mathbf{x}_g)$. Since the uncertainties in $\rho_t(\mathbf{x}_g)$ are so large, even large changes in the parameters λ, k and Φ of the controller did not affect the simulation results.

XV. Conclusions

This paper is concerned with the general area of the robustness of FBLC design to unmodeled dynamics and parametric uncertainties. In cases where unmodeled dynamics can not be neglected by selective modal analysis or singular perturbation arguments, a closer study of the impact of these uncertainties on controller performance is needed. Often counter-intuitive results are reached. It is shown that careful analysis and design of the specific structural model and parametric uncertainties provides robust performance of an FBLC for a wide range of uncertainties. The conclusions depend on the controlled phenomenon; i.e., on the range of frequencies for which it is relevant to have accurate design.

The controller is shown to be stable when one example of structured unmodeled dynamics are added; however, it is important to know whether the controller remains stable when the parameters of these extra dynamics vary. Since it may not

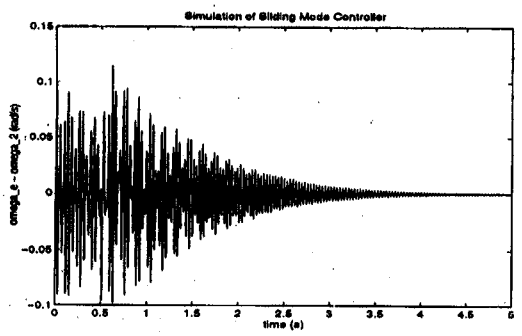

Fig. 35. Plot of $\omega_e - \omega_2$ for a 0.5 s fault. The speed difference multiplied by K_{2eu} dominates the quantity $\rho_t(x_g)$.

be desirable to modify FBLC to improve its performance in the presence of shaft dynamics, it is natural to ask whether the torsional dynamics can interact in such a way as to cause FBLC to become unstable. The stability robustness tests strongly suggest that the answer is no, although the proof of this assertion for all possible combinations of shaft parameters has not been shown. Unfortunately, the computation required to determine stability robustness grows exponentially with the number of uncertain parameters.

The stability robustness of the sliding mode control has a firmer theoretical basis than that of FBLC, although in simulations with torsional dynamics present, sliding control is observed to provide no improvement in performance over FBLC. The uncertainties in the model are of large amplitude and high frequency, and the sliding mode controller is unable to compensate for them. Consequently, like FBLC, the low frequency component of the field voltage is able to provide a reasonable response, although performance is not able to match the results obtained when torsional dynamics are not modeled in the simulations.

REFERENCES

[1] J. W. Chapman, M. D. Ilić, C. A. King, L. Eng, and H. Kaufman, "Stabilizing a multimachine power system via decentralized feedback linearizing control," *IEEE Trans. Power Syst.*, vol. 8, no. 3, pp. 830–839, Aug. 1993.

[2] F. K. Mak, "Analysis and control of voltage dynamics in electric power systems," Ph.D. dissertation, Univ. Illinois, Urbana-Champaign, 1990.

[3] D. Walker, C. Bowler, and R. Jackson, "Results of subsynchronous resonance test at mohave," *IEEE Trans. Power Apparatus Syst.*, vol. PAS-94, no. 5, pp. 1878–1886, 1975.

[4] P. Kokotović, H. K. Khalil, and J. O'Reilly, *Singular Perturbation Methods in Control: Analysis and Design.* Orlando, FL: Academic, 1986.

[5] E. Allen, "Effects of torsional dynamics on nonlinear generator control," Master's thesis, Massachusetts Inst. Technol., Cambridge, 1995.

[6] I. J. Pérez-Arriaga, G. C. Verghese, and F. C. Schweppe, "Selective modal analysis with applications to electric power systems, Part I: Heuristic introduction," *IEEE Trans. Power Apparatus Syst.*, vol. PAS-101, no. 9, pp. 3117–3134, 1982.

[7] A. Sáiz-Chicharro and I. J. Pérez-Arriaga, "Selective modal analysis of subsynchronous resonance," in *Proc. 9th Power Syst. Computation Conf.*, 1987.

[8] P. Anderson, B. Agrawal, and J. Van Ness, *Subsynchronous Resonance in Power Systems.* New York: IEEE, 1990.

[9] R. Schulz, "Synchronous machine modeling," IEEE Publication 75 CH0970-4-PWR, 1975.

[10] A. V. Oppenheim, A. S. Willsky, and I. T. Young, *Signals and Systems.* Englewood Cliffs, NJ: Prentice-Hall, 1983.

[11] M. Ilić and J. Zaborsky, "Dynamics and control of the large electric power systems," Massachusetts Inst. Technol., 6.686 class notes, 1994.

[12] B. R. Barmish, *New Tools for Robustness of Linear Systems.* New York: Macmillan, 1994.

[13] J. J. E. Slotine and W. Li, *Applied Nonlinear Control.* Englewood Cliffs, NJ: Prentice-Hall, 1991.

Eric H. Allen was born in Dover-Foxcroft, ME, on April 29, 1971. He received the B.S. degree in electrical engineering from Worcester Polytechnic Institute and the S.M. degree in electrical engineering from the Massachusetts Institute of Technology in June 1993 and February 1995, respectively. He is currently working toward a doctorate degree at the Massachusetts Institute of Technology, Cambridge.

His research interests include nonlinear control and secondary level power system control in a deregulated utility environment.

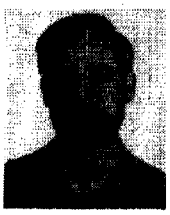

Jeff W. Chapman received the B.S.E.E. degree from the University of California at Santa Barbara and the S.M. degree in electrical engineering with emphasis in power systems at the Massachusetts Institute of Technology, in 1990 and 1992, respectively. He is currently a Ph.D. student at the Massachusetts Institute of Technology.

His research interests include power systems control and nonlinear control.

Marija D. Ilić received the Dipl.Eng. degree and the M.E.E. degree from the University of Belgrade, Yugoslavia, in 1974 and 1977, respectively, and the M.Sc. and D.Sc. degrees in systems science and mathematics from Washington University, St. Louis, MO, in 1979 and 1980, respectively.

She has since been actively involved in teaching and research in the area of large scale electric power systems at Cornell University, the University of Illinois at Urbana-Champaign, and the Massachusetts Institute of Technology, Cambridge. She is presently a member of the Massachusetts Institute of Technology Department of Electrical Engineering and Computer Science, where she holds the position of Senior Research Scientist. She is also a Member of the Laboratory for Eletromagnetic and Electronic Systems (LEES) and an Associate Member of the Center for Energy and Environmental Policy Research (CEEPR) at MIT. Her research interests include control and network theory applications to large scale power systems.